Climate Dynamics (2003) 20: 537–554
DOI 10.1007/s00382-002-0291-3

E. Xoplaki · J.F. González-Rouco · D. Gyalistras
J. Luterbacher · R. Rickli · H. Wanner

Interannual summer air temperature variability over Greece and its connection to the large-scale atmospheric circulation and Mediterranean SSTs 1950–1999

Received: 21 December 2001 / Accepted: 20 September 2002 / Published online: 12 December 2002

Abstract The interannual and decadal variability of summer (June to September) air temperature in the northeastern Mediterranean is analysed for the period 1950 to 1999. Extremely hot and cool summers are illustrated by means of composite analysis. The combined influence of the large-scale atmospheric circulation and thermic predictors on local temperature is assessed by means of an objective approach based on empirical orthogonal functions and canonical correlation analysis. Monthly values of sea level pressure, geopotential heights, atmospheric thickness and Mediterranean sea surface temperatures are used as predictor fields and air temperature from 24 observational sites spread over Greece and western Turkey constitute the predictand variable. Results indicate that more than 50% of the total summer temperature variability can be explained linearly by the combination of eight large-scale predictor fields on two canonical correlation modes. The first canonical mode is related to a more meridional circulation at the upper tropospheric levels, which favours local land–sea contrasts in the associated local temperature pattern. Variations of this mode are found to be responsible for the occurrence of extreme events and decadal trends in regional temperature, the latter being characterized by a cooling in the early 1960s and a warming in the early 1990s. The second canonical mode pictures variations in the intensity of the zonal circulation over the Atlantic area that drive temperature anomalies affecting mainly the Aegean Sea and the west of Greece. Our results suggest the potential of statistical downscaling for Greek summer temperature with reliable climate forecasts for planetary-scale anomalies.

E. Xoplaki (✉) · D. Gyalistras · J. Luterbacher · H. Wanner
Institute of Geography,
University of Bern, Hallerstrasse 12,
3012 Bern, Switzerland
E-mail: xoplaki@giub.unibe.ch

E. Xoplaki
Department of Meteorology and Climatology,
University of Thessaloniki, Greece

J.F. González-Rouco
Institute for Coastal Research,
GKSS, Geesthacht, Germany

J.F. González-Rouco
Departamento Astrofisica y Ciencias de la Atmosfera,
Universidad Complutense de Madrid,
Madrid, Spain

J. Luterbacher · H. Wanner
National Competence Center of Research in Climate,
University of Bern, Bern, Switzerland

R. Rickli
Meteotest, Bern, Switzerland

1 Introduction

Present-day weather conditions affect natural, social, and economic systems in Europe in ways that reveal sensitivities and vulnerabilities to climate change. Southern Europe, in particular, is considered to be one of the most vulnerable regions (IPCC Climate Change 2001a).

The Mediterranean region lies in an area of great climatic interest since it is influenced by some of the most relevant mechanisms of the global climate system: the North Atlantic Oscillation, the South Asian Monsoon, the Siberian High Pressure System and the Southern Oscillation (Corte-Real et al. 1995; Ribera et al. 2000; Maheras et al. 2001). Warm dry summers and the cool rainy winters are the main characteristics of the Mediterranean climate.

The Aegean Sea and the surrounding lands, Greece and western Turkey, constitute the northeasternmost part of the Mediterranean basin. The terrain is rugged and mountainous with sharp orographic gradients. As a consequence, the region shows a variety of climatic zones (pure Mediterranean, marine Mediterranean, Central European and Alpine). The atmospheric circulation, the latitude, the altitude, the orography, and the

land–sea interactions exert a characteristic influence on air temperature distribution (Lolis et al. 1999). Summer air temperatures are an issue of great concern, since their variability and extremes have important economic and social implications. Climate is the main factor that determines the tourism potential of a region (Matzarakis 1999). June to September tourism contributes to around 5% of the Greek GDP (Gross Domestic Product; source: Greek National Tourism Organization, http://www.gnto.gr/). Heat waves, like those during the summers of 1987 and 2000 with disastrous consequences for humans and forests, are likely to reduce the traditional peak summer demand at Mediterranean holiday destinations (IPCC Technical Summary 2001). In addition, heat waves have been associated with short term increases in all causes of mortality (Kovats et al. 1999) as well as with exacerbation of air pollution and extension of vector borne diseases (IPCC Policy Makers 2001). Water shortage problems caused by the shortening of the growing season for different crops have also been reported (IPCC Policy Makers 2001).

Since ancient times, human action has greatly transformed the natural environment in Greece. The Greek National Committee for Combating Desertification reported that as a result of the over-exploitation of the soil, water and vegetation and vegetation resources, desertification is already a realistic threat in the country (GNCCD 2000).

The climate change debate has also shown concern regarding this issue. The IPCC published new projections concerning future emissions in their Special Report on Emissions Scenarios (SRES; IPCC Emissions Scenarios 2000). According to this report, Southern Europe is one of the land areas that will experience a sizeable reduction in the amount of rainfall during the twenty first century. In addition, between the present day and the end of the twenty first century summer warming ranging between 2 and 4 °C for the different scenarios is predicted (IPCC Emissions Scenarios 2000). From nine climate models under the A2 and B2 emissions scenarios reviewed by the IPCC (2001b), Mitchell et al. (2002) report summer temperatures increases over Greece between 2070 and 2099 of the order of 2 to 5 °C compared to the 1961–1990 period. Mitchell et al. (2002) also forecast distinctively lower summer precipitation over Greece for the last decades of the twenty first century.

Many studies have reacted to these forecasts by focusing on recent air temperature trends. Low summer air temperatures for many Greek weather stations have been reported from the end of the 1950s until the beginning of the 1980s, with lowest values in the 1970s (Metaxas et al. 1991; Bartzokas and Metaxas 1995; Proedrou et al. 1997). This relatively cool period was followed by the ''well-known'' Northern Hemisphere warming of the late 1980s that was lagged in the eastern Mediterranean compared to the whole hemisphere (Giles and Flocas 1984; Bartzokas et al. 1994; Maheras and Kutiel 1999). Between the late 1960s and the early 1990s, Turkish coastal regions were characterised by cooler conditions, mainly during summertime (Türkeş et al. 1995, 2002; Kadıoğlu 1997; Tayanş et al. 1997).

It has been long clearly understood that monthly air temperature anomalies are, to a large extent, determined by the monthly mean geopotential height fields for mid tropospheric levels (Namias 1948). Thus, advective processes exerted by the atmospheric circulation are a crucial factor controlling regional changes of temperature (Trenberth 1990, 1995; Hurrell 1995; Hurrell and van Loon 1997; Slonosky et al. 2001; Slonosky and Yiou 2002). The large-scale interrelation between the circulation and air temperature arises because they are both associated with change in the quasi-stationary planetary waves and other factors, including the role of advection given by the mean flow and the planetary waves. This influence is stronger during winter but weaker during summertime due to the heat capacity of the underlying surface (Trenberth 1995). Low and high frequency variations in local air temperatures (year-to-year, decade-to-decade) are far from uniform but occur in distinctive large-scale patterns (Trenberth 1995).

For the whole Mediterranean basin, positive sea level pressure (SLP) trends during summer have been detected (Sahsamanoglou and Makrogiannis 1992, for 1950–1988; Reddaway and Bigg 1996, for 1946–1987; Maheras et al. 1998, for 1950–1994; Xoplaki 2002, for 1950–1999). Maheras et al. (1998) also reported that for the 500 hPa level, positive trends characterise the Western Europe and western Mediterranean. In addition, Wanner et al. (1997) and Schönwiese et al. (1998) found a statistically significant upward trend, for the last few decades in the surface pressure and the geopotential height over the eastern Atlantic and most of continental Europe, including Greece. Xoplaki (2002) found for both winter and summer 500 hPa and 1000 hPa geopotential heights upward trends from the tropics to the midlatitudes. The most significant positive trends are found over the European continent west of around 30°E covering a large portion of the Mediterranean area. The trends are more distinct at the 500 hPa level. Trends towards lower geopotential heights are prevalent over the subpolar regions.

In some specific cases, the local warming trends have been related to urban heat island effects (Katsoulis and Theoharatos 1985; Metaxas et al. 1991; Bartzokas and Metaxas 1995; Türkeş et al. 2002) and in a few cases, changes in the large-scale circulation have been invoked to explain summer air temperature trends. For instance, the cooling at the beginning of the 1980s has been attributed to local circulation changes that favoured stronger and more frequent northerly winds in the Aegean region (Bartzokas and Metaxas 1991; Metaxas et al. 1991; Reddaway and Bigg 1996), or to the increase of the northerly meridional circulation (Kutiel and Maheras 1998). In spite of these attempts, more efforts are needed, to relate the large-scale circulation variability that affects Greek climate including the 1990s data, in order to understand the summer climate variability and trends in this area.

This study tries to make an advance in the understanding of the Greek and western Turkish summer climate for the period 1950–1999 by directly assessing the relationship between the large-scale circulation at different levels (sea level pressure, geopotential height fields, thickness fields and Mediterranean sea surface temperatures) and regional summer air temperatures with an optimised methodology. The relevance of the large-scale atmospheric circulation, thickness fields and Mediterranean sea surface temperatures (SSTs) onto summer surface air temperature is quantified by identifying the physical mechanisms responsible for interannual and decadal air temperature variability over Greece and western Turkey. The large-scale state for cool and warm summers is described and related to the relevant modes of large-scale climate variability.

In Sect. 2, a brief description of data sets and their preparation is given. Methods are described in the third section. Anomaly composites of the fields of SLP, geopotential height fields, thickness patterns and Mediterranean SSTs related to cool and warm Greek summers are given in Sect. 4. This section also includes the results of the canonical correlation analysis (CCA) between Greek surface air temperature and the large-scale geopotential height, thickness and SST fields. The discussion and the conclusions are presented in Sects. 5 and 6, respectively.

2 Data and data preparation

Several data sets were used in this study: station air temperature, gridded sea level pressure, gridded geopotential heights at different levels and thickness fields as well as Mediterranean SSTs.

Monthly air temperature data for 21 Greek stations, equally distributed over the whole country, stem from the National Meteorological Service. The Greek air temperature data can be considered as homogeneous (Xoplaki et al. 2000). The data have been checked with the methods described in Xoplaki et al. (2000). In addition, three Turkish stations located along the Aegean coast were obtained from the National Climatic Data Center (NCDC) Global Historical Climatology Network (GHCN2) (Vose et al. 1992; Peterson and Vose 1997) and included in the study. These data have been quality checked (Peterson et al. 1998). The geographical distribution of these 24 stations together with the topography of the area and the corresponding summer mean temperatures is presented in Fig. 1a.

The 6-hourly gridded (2.5° latitude × 2.5° longitude) SLP data and geopotential heights at different levels (1000 hPa, 850 hPa, 700 hPa, 500 hPa and 300 hPa) were taken from the NCEP/NCAR reanalysis data sets (Kalnay et al. 1996; Kistler et al. 2001). Monthly mean values of SLP and geopotential heights were computed from the 6-hourly data. Thickness fields (1000–700 hPa; 700–500 hPa and 500–300 hPa) were derived from the corresponding geopotential height data.

The monthly SST data originate from the Global Ice Sea Surface Temperature (GISST) data set, version 2.3b, which updates GISST 2.2 described in Rayner et al. (1996) (http://www.badc.rl.ac.uk/). The spatial resolution is 1° latitude × 1° longitude.

The selected period of our analysis covers the summer months (June, July, August and September) of the 1950–1999 interval. The difference, in comparison to the common climatological studies which define summer as June, July and August, stems from the fact that the September air temperature over the area studied, in terms of its mean and variability (not shown), behaves more like a summer month than an autumn month.

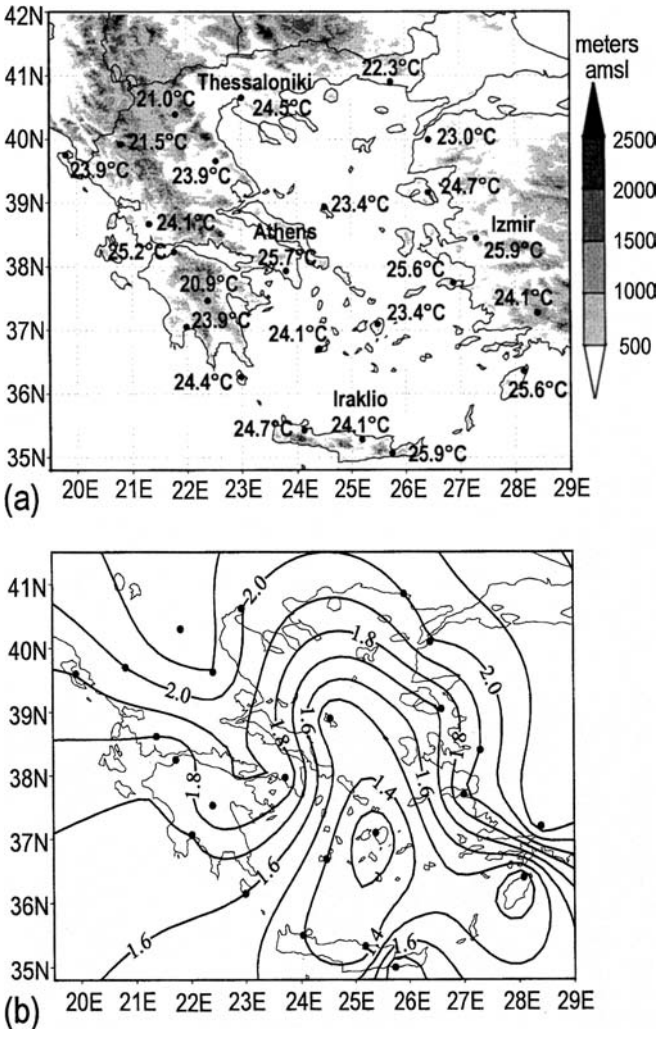

Fig. 1 **a** Geographical distribution of the 21 Greek and three western Turkish stations. The mean summer air temperature (°C) of the stations is given together with the topography of the area. **b** Summer air temperature standard deviation of the Greek and western Turkish stations

The surface climate is often sensitive to minor shifts in large-scale atmospheric patterns (e.g., Yarnal and Diaz 1986). In order to isolate the characteristics of atmospheric variability regarding the Greek and the western Turkish area, a spatial window for the large-scale atmospheric parameters has been defined according to the highest Pearson product moment correlation between the first empirical orthogonal function (EOF) of the summer Greek air temperature and the gridded large-scale Northern Hemisphere geopotential height fields. It turned out that the area extending from 60°W to 80°E and 20°N to 80°N, including 1423 grid points, provides the most valuable atmospheric information connected to the summer air temperature conditions. For the SST, we chose 1102 grid points covering the entire Mediterranean and the Black Sea (9.5°W–44.5°E, 30.5°N–49.5°N).

Prior to all analyses, the annual cycle has been removed from all station and grid point time series by subtracting from each monthly value the respective month's 1950–1999 long-term mean. Summer mean anomalies for a particular year were computed by averaging the months June through September. Due to the almost equal distribution of the stations over the investigated area no weighting was applied on the temperature data.

During the second half of the twentieth century, the concentrations of various radiatively active gases in the atmosphere have strongly increased, such that it is very likely that the global and regional climate was not stationary throughout our analysis interval (IPCC Climate Change 2001a). Therefore, in order to remove possible first-order effects of anthropogenic climate change, the EOF and CCA analyses were applied to detrended anomaly data. The linear trend, which was determined by the regression analysis at each grid point or station time series, was removed from the SLP, geopotential heights, thickness fields, SSTs and station air temperature data.

For the transformation of the Greek and western Turkish station air temperature data into a field analysis, the Kriging interpolation scheme (Brown and Eischeid 1992) was used, where the contour lines give an "optimum" between smoothing in space and realistic reproduction of the station data (Schönwiese et al. 1994) (See Figs. 1b, 3i, 4i, 6i and 7i). However, caution should be exercised (in interpretation) in regions without data, or where the station-to-station distances are large, or where orography is an important factor.

3 Methods

3.1 Weighted mean and anomaly composites

In the first part of the analyses, the composite technique is used to extract information regarding the large-scale climate signal contained in the Greek summer air temperature. This technique attempts to identify coherent structures in the geopotential height, thickness and SST fields that are associated with anomalous summer air temperatures over the whole Greek and the western Turkish area. An anomaly time series representative of the areal mean air temperature anomalies $\bar{x}(t)$ was constructed using the equation $\bar{x}(t) = \sum_{i=1}^{n} (k \cdot x_i(t)/\sigma_i)$, where t is time, $x_i(t)$ represents the monthly air temperature anomalies of each station relative to the reference period 1950–1999, the factor k is $k = 1/\sum 1/\sigma_i$ and σ_i is the standard deviation of each individual station.

After the calculation of the summer weighted mean air temperature anomalies, the ten warmest and the ten coolest summers were selected for the composite analysis. The compositing was conducted by calculating the averaged seasonal mean of the ten warmest and the ten coolest summers minus the averaged seasonal mean for the period 1950–1999 of the large-scale atmospheric fields as well as for the SST fields, respectively. The significance of the anomaly composites was assessed by Welch's modified t-test (Welch 1937).

3.2 Canonical correlation analysis (CCA) in empirical orthogonal functions (EOF) space

Canonical correlation analysis is a multivariate technique for analysing associations between a set of independent variables (predictors) and a set of dependent variables (predictands) (Hotelling 1935, 1936). The underlying assumption in the computations of the CCA is that the relationships between variables are linear (Glahn 1968; Levine 1977).

The CCA selects pairs of spatial patterns of two space/time-dependent variable sets such that the (time dependent) pattern amplitudes are optimally correlated (Preisendorfer 1988; Wilks 1995; von Storch and Zwiers 1999). The canonical correlation coordinates (i.e. the intensities of the modes) describe the strength and the sign of the corresponding patterns for each realization in time. Since the canonical series are normalised to unit variance, the canonical correlation patterns are expressed in the units of the variable they represent and they indicate the "typical" strength of the mode of covariation described by the patterns. The correlation between the canonical coordinates measures the degree of association between the two canonical patterns (von Storch and Zwiers 1999).

Prior to the CCA, the original data are projected onto their empirical orthogonal functions. An advantage of using the EOFs in the CCA is that the input data are independent (orthogonal functions). In addition, it is possible to retain only the few first EOFs, which serves as a data filtering procedure that eliminates the noise of the fields involved by discarding the high-index EOFs. These usually correspond to poorly organised small-scale features of the fields involved. Another advantage is that it reduces the dimensionality of the problem, an issue that is not irrelevant in terms of computation, particularly regarding the multicomponent CCA analysis described later.

The selection procedure for the number of EOFs from the predictand and the predictor fields for the subsequent CCA is of great importance (von Storch and Zwiers 1999; Livezey and Smith 1999a, b; Smith and Livezey 1999). On the one hand, too few EOFs will omit part of the significant signal, thus resulting in a poorer prediction of the overall CCA model. On the other hand, using too many EOFs will fit the statistical models too strongly to particular data sets considered, and most likely resulting in missing an adequate description of the underlying process.

There is not a single clear criterion that can be used to choose the number of principal components that are best retained in a given circumstance. Two graphical rules based on the relative magnitudes of the eigenvalues, are the scree graph (Cattell 1966) and the log-eigenvalue (LEV) diagram (Craddock and Flood 1969). Another criteria are the Kaiser criterion (Kaiser 1960), the rule N (Preisendorfer et al. 1981) and North's rule of thumb (North et al. 1982a). In this study, the selection of the number of EOFs was made with the use of the scree graph.

In order to account for the latitudinal distortions, each grid point of the geopotential height field anomalies was weighted by the square root of cosine of the latitude (ϕ) (North et al. 1982b). This has the effect of weighting the variance for each grid point by the size of the geographical region it represents. The detrended regional air temperature time series were scaled to unit variance, such that all stations in the subsequent analysis have the same weight.

CCA experiments have been conducted with summer temperature as the dependent variable in two different ways: (1) CCA experiments with single geopotential height and thermal fields as predictors, and (2) CCA experiments with multicomponent predictors (Gyalistras et al. 1994). In both cases, a varying number of EOFs has been considered for the predictor and predictand variables. The second set of experiments was conducted in order to investigate the covariability between all eight geopotential height and thermal fields and the station air temperature. This has the advantage of enabling the study of the relationship between the summer mean air temperature and the joint information from various atmospheric and SST fields, rather than just a single field. Here, only simultaneous connections between the different fields and summer temperature were considered. No lead or lag relationships were taken into consideration.

3.3 The cross-validated CCA

Cross-validation is a statistical procedure used, in order to reduce the problem of artificial skill produced by the overfitting of random variability in the data (Barnett and Preisendorfer 1987; Michaelsen 1987; Ward and Folland 1991; Elsner and Schmertmann 1994; von Storch and Zwiers 1999). Cross validation is a resampling technique, where the available data are repeatedly divided in validation and verification data subsets. It is a generalisation of the common technique of omitting in the model building procedure a few observations (calibration) and then testing the model with the omitted observations (validation) (Michaelsen 1987; Wilks 1995; von Storch and Zwiers 1999). The cross validation model is developed on a data set that has almost the same number of degrees of freedom as the original and for each observation independent predictions are made (Michaelsen 1987).

For our analysis, each month was withheld once from the data set and the calculations were performed without it. The model is

fitted to the retained data (199 summer months) and used to make specification of the withheld data (von Storch and Zwiers 1999). This process was then repeated for each summer month in the record.

It should be emphasised that replication techniques (like cross-validation) are especially (if not critically) important to use when performing a CCA. All multivariate analyses capitalize on sampling error, but CCA is particularly susceptible to biases in the samples (Kier 1997; von Storch and Zwiers 1999).

The correlation (ρ) between predictions and observations and the Brier skill score (β) (von Storch and Zwiers 1999) have been used as measures of the performance of the statistical downscaling approach. The correlation provides a measure of time concordance in the series, while the Brier score allows for a measure of the explained variance by the model (Livezey 1995). The Brier score is defined as $\beta = 1 - \left|S^2_{FP}/S^2_P\right|$ where $S^2{}_{FP}$ represents the variance of the error of the forecasts F to the reference predictands P and S^2_P stands for the variance of the predictand variable P. Thus, for predictions with errors which variance ranges on the order of the variance of the predictand β will be close to 0 or negative and for predictions with a small amount of error, β tends to 1 (von Storch and Zwiers 1999).

4 Results

Figure 1b shows the standard deviation of the summer mean air temperature at each station for the period 1950–1999. Its distribution follows the topography of the region, with low values (smaller variability) over the sea/islands in the central-south Aegean area and high values (higher variability) over the mainland in north and central Greece, following the Greek mountain chain of Pindos. The moderating effect of the sea on temperature is therefore well illustrated by this figure. However, it should be stressed that due to the lack of stations at the corners of the chosen geographical window, caution should be exercised on the interpretation in these particular regions.

The spatial heterogeneity of the temperature variability presented in Fig. 1b is taken into account for the calculation of the weighted summer mean temperature anomalies, which are presented in Fig. 2a. For the mean summer as well as for the individual months (not shown), the positive air temperature deviations tend to be larger than the negative ones. However, the number of summers since 1950 with negative deviations is higher than of those with positive deviations.

The beginning of the 1950s and the end of the 1990s present the two clusters with warmer than normal summer air temperature. The average of the four long time series of Thessaloniki, Larissa, Athens and Patra, going back to the beginning of the twentieth century, indicate that the 1920s and 1940s were even warmer (Fig. 2b). The warmest summer was in 1999 with a difference of 1.46 °C from the long-term 1950–1999 mean. It should be noted that all four summer months contributed with large positive anomalies to this warm summer. The second part of the 1970s and the early 1980s were characterised by cooler summers. The summer of 1976 was the coolest over the last 50 years with a negative deviation of 1.62 °C from the long-term

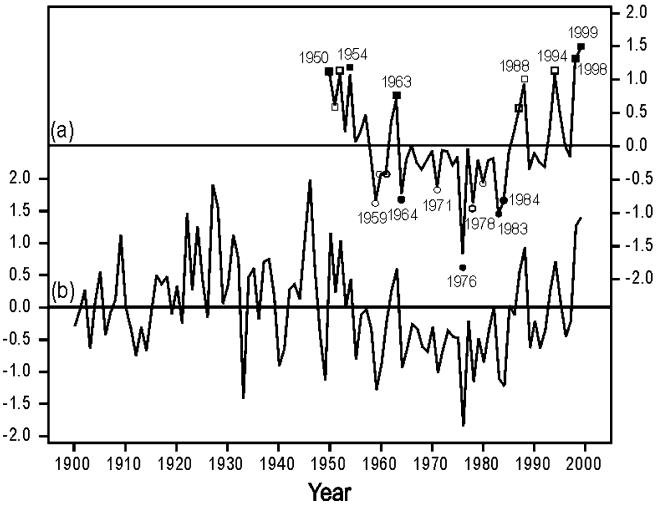

Fig. 2 **a** Spatially weighted mean of summer (JJAS) air temperature anomalies from Greece and western Turkey from 1950–1999 (*solid line*). *Circles*: 10 coolest summers. *Squares*: 10 warmest summers. *Solid symbols* correspond to the extreme summers, in which at least three single months are characterised by "extreme" air temperature conditions. **b** Spatially weighted mean of summer (JJAS) air temperature anomalies (Thessaloniki, Larissa, Athens and Patra) from 1901–1999 (*solid line*)

1950–1999 mean. All individual summer months contributed to the cool conditions.

No significant linear trend in the averaged summer months (J,J,A,S) and entire summer mean air temperature could be detected. The calculated mean trend is 0.28 °C/50 yrs for June, 0.03 °C/50 yrs for July, –0.32 °C/50 yrs for August, –0.25 °C/50 yrs for September and 0.003 °C/50 yrs for the entire summer, respectively. The most remarkable features concerning trends are on decadal time scales: the cooling trend at the beginning of the 1960s and the warming at the end of the 1980s. These are present in the time series of every station.

Based on Fig. 2a we selected the ten coolest and ten warmest summers between 1950 and 1999 to construct the temperature anomaly composites. These anomaly composites are related to the large-scale atmospheric circulation at different levels as well as to the thickness and SST fields. The results will be presented in the following section.

4.1 Anomaly composites of warm and cool summers

This section describes the spatial variability of anomalous cool and warm summers over Greece and western Turkey. Some insight is also given into the large-scale climate anomalies connected to the summer air temperature extremes.

Figure 3 shows the anomaly (1950–1999 mean subtracted) composites of the SLP, the geopotential heights at different levels, the thickness patterns and the SSTs as

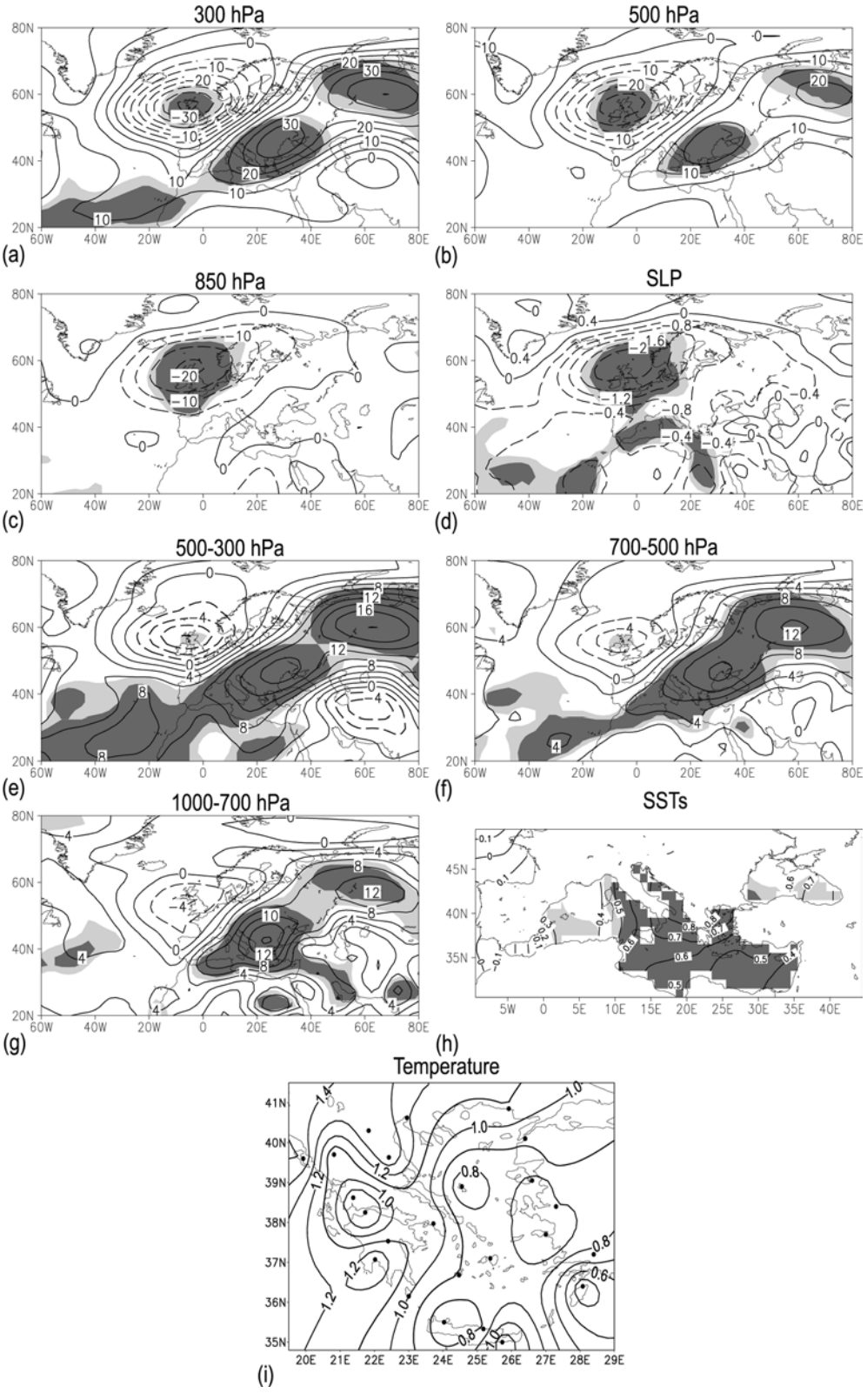

Fig. 3 Anomaly composites of **a–c** geopotential heights, **d** SLP, **e–g** thickness at three levels, **h** Mediterranean SSTs and **i** station air temperature anomalies for the ten warmest summers. Significant areas at the 90% and at the 95% confidence level are *shaded* in *light* and *dark grey* colour, respectively

well as the local surface temperature for the ten anomalous warm summers derived from Fig. 2a.

The air temperature anomaly composite reveals a monopole pattern with overall significant positive values. The isotherms follow approximately the morphology of the area. Lowest anomalies are prevalent over the Aegean Sea (see also Fig. 1b) while over the mainland high temperature variability dominates.

The geopotential height anomaly composites related to extreme warm summers (Fig. 3a–d) indicate at all levels significant negative anomalies centred over the northern British Isles. The extent of significant areas increases from the 300 hPa to the SLP. Significant positive large-scale anomalies are represented as a long belt extending diagonally from the southeastern to the northwestern part of the spatial window covering the whole Mediterranean area. These positive anomalies decrease towards lower levels and disappear completely at the 850 hPa level (Fig. 3c). At sea level, even significant negative pressure values are prevalent over the Mediterranean.

Anomalously warm air temperatures over Greece (Fig. 3i) are also associated with anomalies in the thickness levels (Fig. 3e–g) with negative values over northwestern Europe and the southeastern part of the window (though not significant). Large-scale significant positive anomalies on all thickness levels dominate from the southern North Atlantic over the Mediterranean and Central Europe to Russia.

Positive SST anomalies (Fig. 3h) cover the entire Mediterranean. However, these anomalies are only significant in the central and eastern part.

The anomaly composites related to cool summers for Greece and western Turkey are shown in Fig. 4. The anomaly composite of the ten coolest summers within the period 1950–1999 reveals a similar spatial distribution as in the warm case, though reversed. All stations indicate significant negative temperature anomalies (Fig. 4i). The areas with significant negative geopotential height anomalies (Fig. 4a–d) expanding from Greece to Russia are less accentuated and smaller in magnitude compared to the warm anomaly composites. This seems to be in agreement with the smaller amplitude of the cold temperature anomalies in comparison with the warm anomalies in Fig. 2a.

As for the warm anomaly composites, a tripole of anomalies is discernible in all the thickness charts (Fig. 4e–g). However, there are only small significant areas. Significantly cooler air over Greece is roughly limited to the first 6 km (500 hPa level).

The SST anomaly composite (Fig. 4h) presents a monopole pattern with negative sign over the entire Mediterranean basin, though this is significant only east of 12°E. Interestingly, in both the warm and the cold composite cases, the SSTs tend to show higher values closer to the area of positive anomalies in geopotential height and thickness fields. Moreover, SSTs in the vicinity of Greece are lower than the atmosphere surface temperatures in the warm case and the opposite is valid for the cold case.

4.2 CCA in EOF space

Table 1 gives a summary of the different EOF/CCA analyses of the summer Greek air temperature, the SLP, the large-scale geopotential height fields, and the thickness fields as well as the Mediterranean SSTs of the period 1950–1999. The first column contains the predictors used for the single-component and the multicomponent CCA exercises. The second column presents the number of the predictor EOFs (large-scale geopotential height fields, thickness fields, SSTs) retained for the CCA application for each experiment. Accordingly in the third column, the number of the selected EOFs of the predictand (summer temperature) is included. The cumulative variance of the selected EOFs of the predictor data set is shown in the fourth column. The following two columns of Table 1 contain the squared correlation between the canonical correlation coordinates (shared variance of the canonical patterns) for the first and the second CCA pairs, respectively, thus indicating the degree of association between the predictor and predictand fields. Analogously, in the seventh and eighth columns, the explained variance for the summer temperature canonical patterns (predictand) is given. In the ninth column, the total explained variance by the first two CCA pairs for the whole summer temperature field is shown. These values reveal the total proportion of summer temperature explained by the combination of the first two CCA pairs. Finally, the last and the penultimate columns present the performance of the models, in terms of the correlation and the Brier skill score as derived from the cross-validation exercise.

Two different CCA experiments (see methods section) have been conducted. The first approach (Table 1, rows 2 to 9) examines the (characteristic) connection between the summer air temperature and each single large-scale predictor. The second approach (Table 1, rows 10 to 13) describes the combined influence of all eight predictor fields and summer air temperature.

4.2.1 Single-component CCAs

The CCA experiments with single predictors were conducted with the leading eight predictor data EOFs, accounting for between 63.3% (1000–700 hPa thickness) and 91.2% (SSTs) of the total variance and the three leading air temperature EOFs, explaining 81.8% of the summer variability (Table 1). The squared canonical correlations for both the first and second CCA pairs suggest a significant coupling between the corresponding patterns at the interannual time scale.

CCA ranks the resulting pairs of patterns and time series in decreasing order of the canonical correlation. All the single-component and multicomponent experiments provided similar pairs of large-scale patterns and associated regional temperature anomalies, which will be described in the following section. For most experiments, the canonical modes emerged in the same order so that, for instance, the first canonical vector refers always to the same large-scale state. However, in the case of the 500 hPa and 850 hPa geopotential heights as well as SLP, the selected canonical pairs resulted in

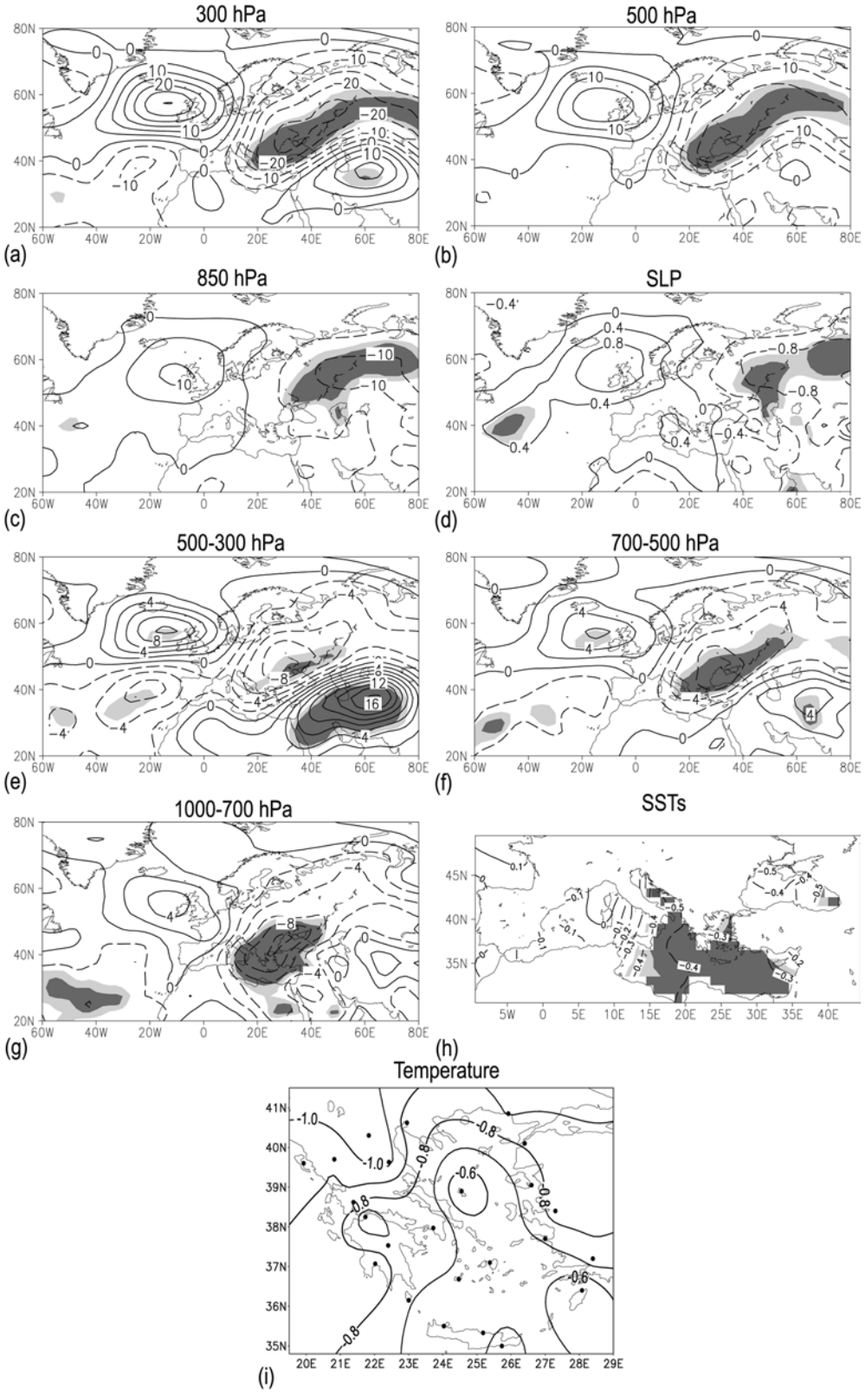

Fig. 4a–i Same as Fig. 3 but for the 10 coolest summers

reverse order compared to the other experiments. Therefore, the reader should bear in mind that for these cases, the second canonical pair is physically equivalent to the first canonical pair in all other experiments. This is highlighted with a star (*) in columns 5 to 8 of the three levels mentioned.

According to the total explained variance of the summer temperature, the most skilful circulation

Table 1 Summary of CCA results

Predictors	No X-EOFs	No Y-EOFs	X-cumulative variance (%)	r^2_{CCA1}	r^2_{CCA2}	Y-explained variance 1 (%)	Y-explained variance 2 (%)	Y-total explained variance 1–2 (%)	Cross-validation	
									Corr.	Brier
300 hPa	8	3	78.2	0.42	0.31	50.1	28.6	30.0	0.59	0.36
500 hPa	8	3	79.8	0.42*	0.28*	32.9*	48.2*	27.5	0.52	0.28
850 hPa	8	3	81.7	0.37*	0.25*	9.8*	71.8*	21.8	0.41	0.19
SLP	8	3	80.1	0.38*	0.24*	18.4*	62.6*	21.8	0.42	0.19
500–300 hPa	8	3	70.9	0.48	0.20	66.8	13.7	34.7	0.62	0.39
700–500 hPa	8	3	69.7	0.47	0.30	71.5	9.2	36.5	0.63	0.41
1000–700 hPa	8	3	63.3	0.72	0.43	72.1	8.7	55.3	0.66	0.42
SSTs	8	3	91.2	0.61	0.40	68.0	13.1	46.9	0.64	0.36
All fields	8	3	76.5	0.64	0.44	68.7	9.7	48.2	0.72	0.53
All fields	16	3	93.0	0.77	0.50	70.2	10.0	59.4	0.74	0.58
All fields	16	2	93.0	0.74	0.49	72.7	9.1	58.2	0.74	0.56

Columns 1 to 3: predictor variable(s), number of predictor(s) and predictand EOFs. Column 4: percentage of accumulated EOFs variance. Columns 5 and 6: squared canonical correlations for the first two CCA modes. Columns 7 and 8: variance each canonical mode accounts for in the predictand. Column 9: total explained variance by both modes. Columns 10 and 11: correlation and Brier score from the cross-validation

predictors are the 300 hPa and 500 hPa geopotential heights. The best thermic predictor is the 1000–700 hPa thickness field followed by the SSTs. Atmospheric thickness and SSTs tend to perform better than circulation predictors.

Cross-validation (last two columns of Table 1) mostly confirms the behaviour of CCA1, with higher (lower) skill on the upper levels for the geopotential (thickness) fields as denoted by the Brier score. The correlations between the cross-validated summer air temperature data and the raw data are significant at the 95% level ($n = 50 \times 4 = 200$ months, $r \geq 0.18$ sign. at the 95% level), even if the autocorrelation between the subsequent summer months is taken into consideration.

4.2.2 Multicomponent CCA

Different CCA experiments with multicomponent predictor fields have been calculated (Table 1): the number of EOFs retained for the various CCAs was 8/16 for the predictor fields (76.5%/93.0% shared variance, respectively) and 3/2 in the case of the summer air temperature (81.8%/77.8% shared variance, respectively).

Only a moderate gain in the total explained variance for the summer air temperature is obtained from the multicomponent CCA (columns 7 to 9 of Table 1). However, the model clearly indicates a better performance in cross-validation (last two columns of Table 1). A parsimonious model, with only two air temperature EOFs, does as well as a model with three air temperature EOFs. The multicomponent CCA indicates that more than 50% of the summer seasonal air temperature variability can be explained by combining all eight predictors.

Figure 5 presents the cross-validated squared correlation between Greek air temperature and the considered predictor fields for each summer month (J,J,A,S) separately. As for the entire summer, the multicomponent CCA model shows better performance than any other model conducted with a single predictor field (Table 1). The thickness layers and the SSTs generally indicate higher skill than the circulation fields. August shows the best predictive skill for each single predictor and the combination of all fields. The relationship between the summer air temperature and

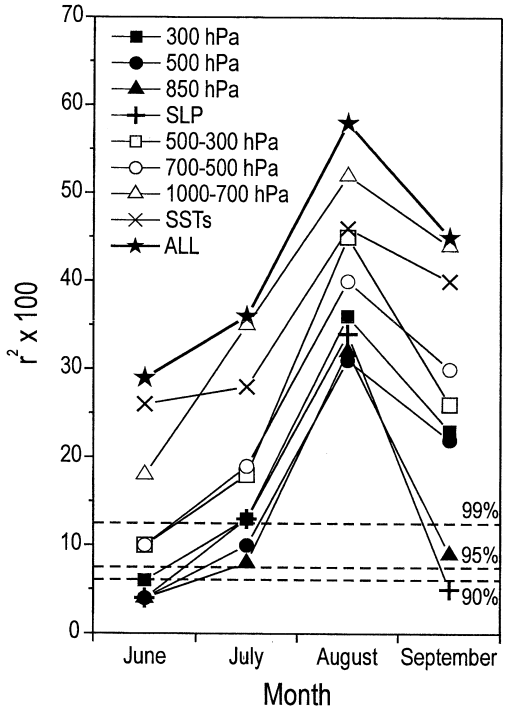

Fig. 5 Correlation coefficients (r^2 multiplied by 100) between cross-validated individual summer month air temperature and raw air temperature data for each single predictor and the multicomponent predictors. The 90%, 95% and 99% significance levels for the correlation coefficients are indicated by *dashed horizontal lines*

the atmospheric predictors and SSTs is rather strong for August, but much weaker for the other months. In addition, here, it is apparent that with regard to geopotential height predictors, skill increases with height while regarding thickness it decreases with height.

The results of the multicomponent CCA, with the highest performance, including all eight predictors are described in the following section with the aim of studying the interannual covariability between the summer air temperature over the Greek and western Turkish areas during the period 1950–1999 and the combined large-scale circulation and thickness fields.

4.3 Maps of CCA results

The following results correspond to the last row of the Table 1. Figure 6 shows the results of the first canonical vector using eight large-scale predictors for local summer air temperature. The retained number of EOFs was 16 for large-scale predictors and two for local air temperature (see Table 1 last row). CCA1 shares 72.7% of the temperature variability and 9.6% of the multicomponent large-scale geopotential height, thickness and SST fields. The squared correlation between the summer air temperature and the predictors is 0.74. The large value implies that this coupled mode reflects more than half of the interaction between the air temperature and the multicomponent atmospheric and thermal anomalies during summer time. In the positive (negative) phase, the anomaly geopotential height patterns at the mid to upper troposphere (500 hPa and 300 hPa levels, respectively; Fig. 6b and a) present a tripole with negative (positive) anomalies centred over the northern British Isles, positive (negative) anomalies over eastern Europe and weak negative (positive) anomalies southeast of the Caspian Sea. At lower levels (Fig. 6c, d), the strong negative (positive) anomaly centre persists though with lower intensity, while the two other anomaly centres vanish. Maximum (minimum) values are expected over land whilst minimum (maximum) air temperature anomalies can be found over the Aegean Sea. An identical tripole structure is prevalent in all thermal atmospheric fields (Fig. 6e–g) with higher intensity at upper layers. Positive (negative) SST anomalies prevail over the whole Mediterranean basin. Higher (lower) SST values (Fig. 6h) are found in the northeastern part, namely over the Aegean and Adriatic seas and the Black Sea, with a gradual decrease (increase) from the central towards the western Mediterranean.

The surface air temperature pattern exhibits positive (negative) anomalies all over the investigated area. The temperature anomalies structure follows the coastline as for the anomaly composites (Figs. 3i, 4i). Maximum values are located over the central and northern parts of Greece as well as over the western Turkish mainland, while minimum values are expected over the meridional Aegean Sea.

The year-to-year variations of the normalised time components of the first CCA pair is presented in Fig. 6j. These normalized time components of the predictand and predictors represent the ''sign'' corresponding to the patterns. For instance, positive (negative) time components for both time series for a specific summer go along with negative (positive) anomalies of the circulation (Fig. 6a–d) and thermal predictors (Fig. 6e–h) over northwestern Europe and positive (negative) anomalies over Eastern Europe and positive (negative) temperature anomalies over Greece (Fig. 6i). The two canonical time series show remarkable variability on the decadal time scale (Fig. 6j). Higher values associated with warm temperature episodes are clustered mainly at the beginning and at the end of the record in a similar fashion to the behaviour of the regional temperature averages (Fig. 2a).

The second CCA pair (Fig. 7) exhibits a squared correlation between the predictor fields and the summer air temperature of 0.49. The shared variance is 9.1% and 8.2% for the summer air temperature and the eight predictor fields, respectively. In the positive (negative) phase, negative (positive) air temperature anomalies are prevalent west of 23°E, whereas above (below) normal air temperatures can be found elsewhere (mainly at stations in the Aegean Sea and western Turkey) (Fig. 7i).

The air temperature CCA pattern is also related to positive (negative) thickness anomalies over the eastern Mediterranean in all layers and cooler (warmer) air temperatures northwest of Greece (Fig. 7e–g). Thus, the area studied marks the transition between the cool and the warm air masses. A similar dipole pattern with positive (negative) values east of 23°E and negative (positive) values over the remaining basin is found in the CCA2 of the Mediterranean SSTs (Fig. 7h).

The second pair of canonical series (Fig. 7j) shows mostly interannual variability with extreme positive values in 1972 and 1995 and negative ones in 1950 and 1982.

5 Discussion

In this study the relationship between the variability of summer surface air temperature over Greece and western Turkey and the state of the large-scale atmospheric circulation and thickness patterns as well as Mediterranean SSTs has been analysed.

Summer in the Mediterranean area is the most difficult season to interpret. This is due to the relatively weak discrimination between the mean monthly charts as a result of the strong persistence of anticyclonic conditions over the Atlantic and Europe and the pronounced stability of the thermal low over the eastern Mediterranean (Maheras et al. 1999).

However, interesting coupling patterns are found both in the composite analysis (Figs. 3, 4) as well as in the CCA (Figs. 6, 7) between local temperature and the large-scale, which provides a first means of explanation for its extremes, interannual variability and decadal trends.

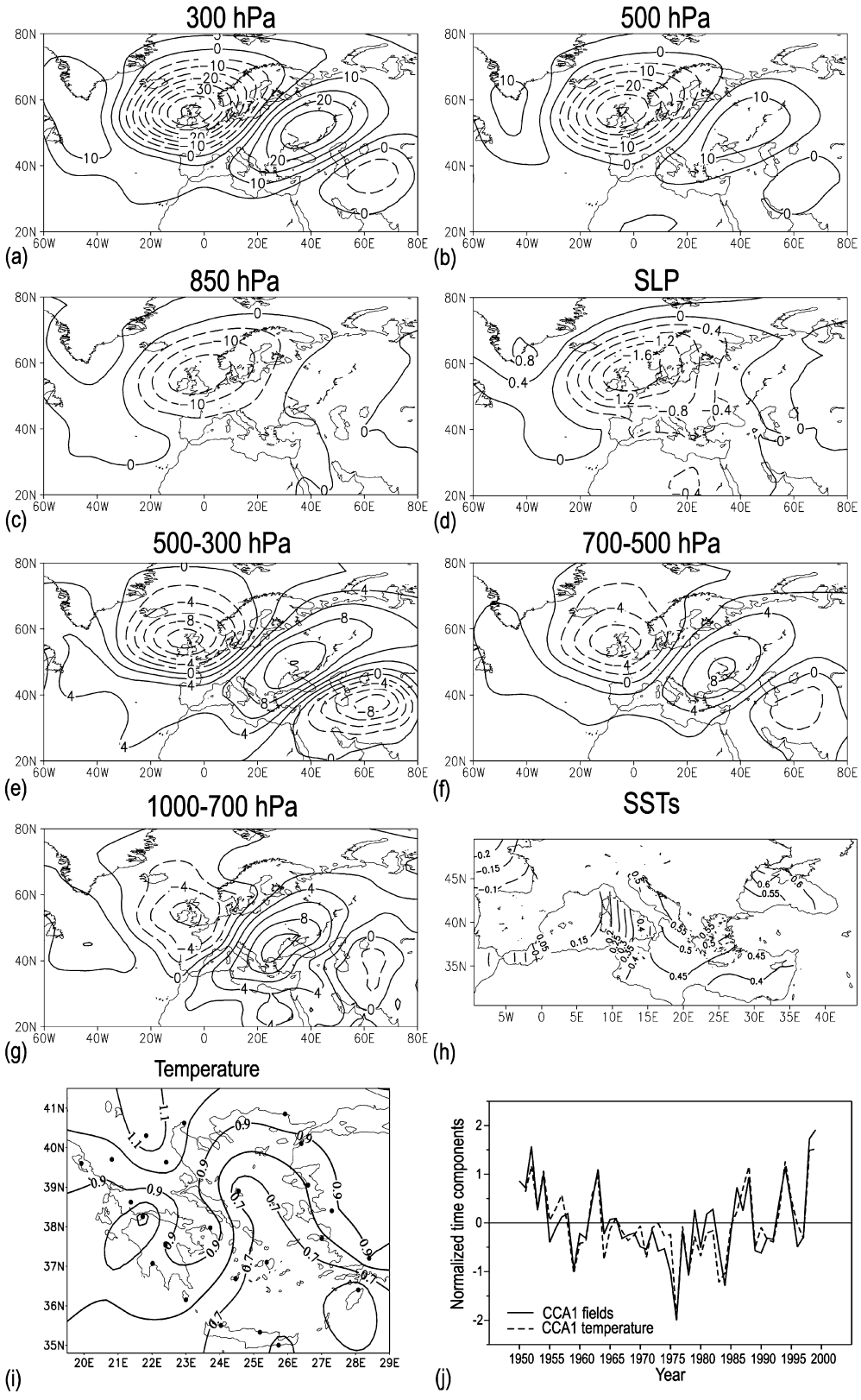

Fig. 6a–d Patterns of the first CCA of each of the eight predictor fields and the Greek and western Turkish temperature. The canonical correlation patterns reflect the typical strength of the signal, with *a–d* the geopotential height anomalies; **e–g** the thickness patterns in geopotential metres (gpm); **h** the SST and **i** the air temperature anomalies in °C; **j** the normalised time components of CCA1

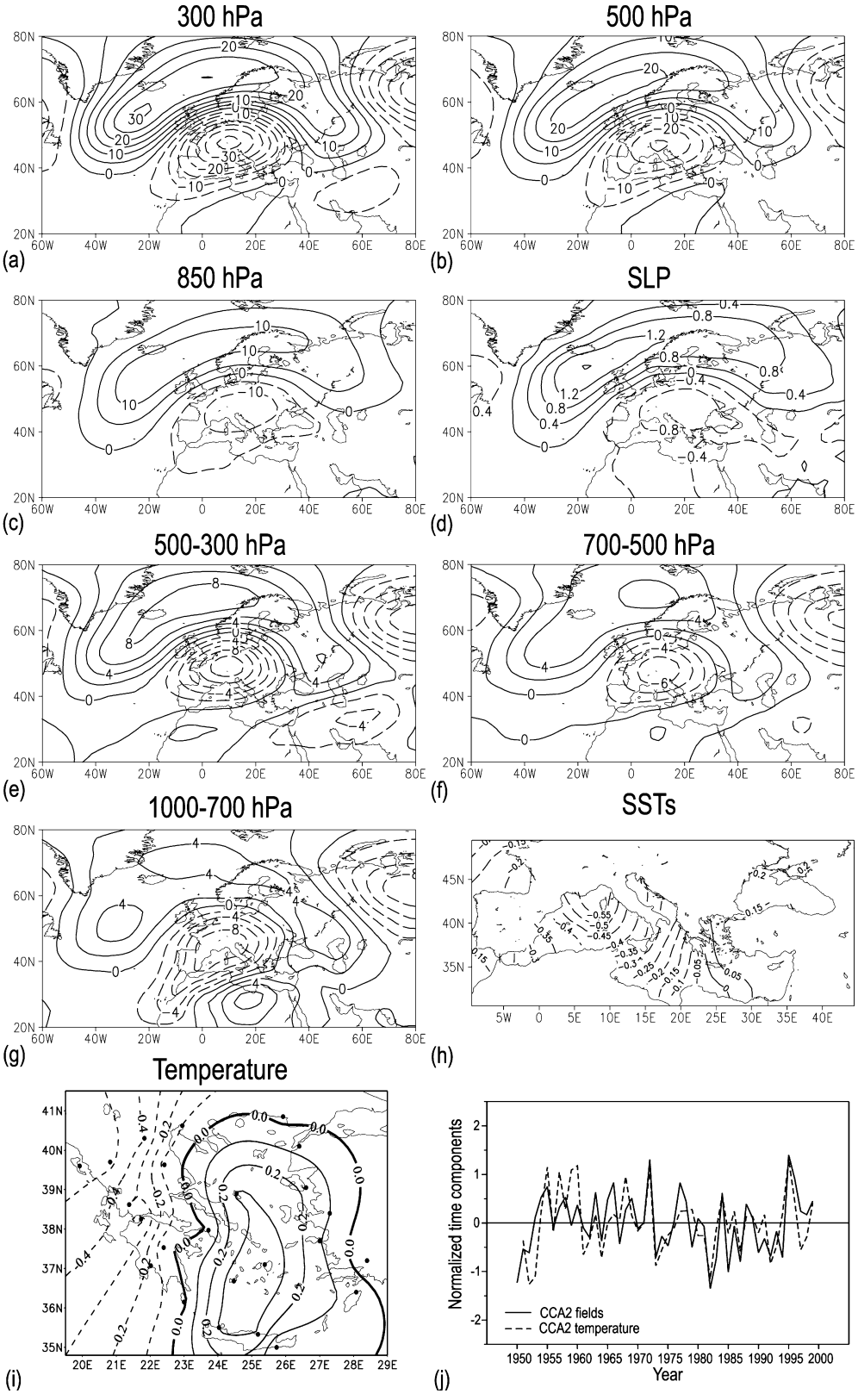

Fig. 7a–j Same as Fig. 6 but for the second CCA

The patterns of the extreme warm and cool summers anomaly composites (Figs. 3, 4) are visually very similar to the positive and negative phase of the first CCA pair, respectively. Therefore, the CCA1 and the composite results are discussed together, while specific features of the "extreme" warm and cool summers are presented at the end of the discussion.

5.1 Coupled CCA1 patterns between Greek summer temperature and combined large-scale atmospheric and thermal fields

The standard deviations of surface summer air temperature in the area (Fig. 1b) show a clear land–sea contrast which is also apparent in the local temperature pattern of CCA1 (Fig. 6i) as well as in the warm and cool composites (Figs. 3i; 4i). The interpretation at the corners of the spatial window should be made with caution due to the lack of information for these regions. The first canonical series of air temperature correlates at 0.99 with the weighted temperature time series shown in Fig. 2b and its highest and lowest values correspond well with those of the extreme states. This canonical component illustrates a mode of large-scale variability that is responsible for 72.7% of the variability of local temperature.

The large-scale variability suggests the influence of a more meridional circulation in the upper levels of the atmosphere, which appears to favour intrusions of warm (cold) air over eastern Europe in its positive (negative) mode.

The circulation in the upper levels can be described as a low index type. In summer months with high positive (negative) values of the first CCA there is an increased frequency of anomalous half-meridional flow from Scandinavia towards the Iberian peninsula, connected with a jet (Polar Front Jet) meandering around a low (high) centred over Great Britain, a high (low) over Eastern Europe and a low (high) to the southeast of the Caspian Sea (Subtropical Jet).

The thickness fields show a persistent structure of anomalies from the surface up to the 300 hPa level, with positive (negative) values in the areas covered by the highs (lows). The SSTs in the positive (negative) phase of the CCA1 reveal a configuration, which follows that of the 1000–700 hPa layer thickness, with lower (higher) temperatures than the overlying atmosphere. The warm high over Eastern Europe and the low southeast of the Caspian Sea are not present at the sea level. Weak anomalous westerly and northwesterly (easterly and southeasterly) winds over the studied region are prevalent during warm (cold) conditions.

In the case of warm anomaly conditions (positive phase of CCA1 and warm composites), warm air dominates over the eastern Mediterranean, connected with an anomalous northeasterly-to-easterly continental flow and subsidence at the upper levels. This leads to increased stability and inhibition of convection resulting in clear skies and maximum insolation conditions. Such a combination favours a temperature structure with land–sea contrasts due to the higher heat capacity of the water masses and faster thermal response of the land.

Maheras and Kutiel (1999) report that the high air temperatures in all seasons over the Mediterranean area are associated mainly with a southerly circulation bringing warm air masses from North Africa or the Sahara desert. This can be seen in the CCA1 patterns as well as in the warm summers composites maps (Fig. 3a–g). The significant positive thickness anomalies throughout the troposphere from the southern North Atlantic to Russia and the warm air advection at the upper troposphere (300 hPa) from the warm African continent to the central Mediterranean and Greece contribute to the atmospheric stability.

In the case of the cold anomaly conditions (negative phase of CCA1 and cool summers anomaly composites), negative temperature anomalies over the eastern Mediterranean are prevalent in the entire air column. The corresponding negative geopotential height anomalies increase with height. They point to a higher frequency of cold air advection in the upper levels. This suggests a higher frequency of shortwave troughs from northerly directions and cut-off lows during the four summer months. Such situations are assumed to be associated with instability therefore convection and increased latent heat flux at the surface, as well as enhanced cloud formation and precipitation. An indirect test for this hypothesis can be the correlation map of the first canonical air temperature series with precipitation provided by the NCEP/NCAR reanalysis (Kalnay et al. 1996; Kistler et al. 2001), shown in Fig. 8. The spatial structure, which arises, shows positive (negative) values indicating wetness (dryness) under the cold lows (warm highs) as an indication for instability (stability). This supports the assumption of convection and cloud formation. Convection contributes to further cooling of the surface and cloud formation, and can also have an indirect cooling effect in the convection areas. However, it has to be pointed out, that the cloudiness as well as the short- and longwave radiation during cool summers and single summer months is not statistically different from hot summers over Greece (not shown). This is an indication of short-lived disturbances connected with thunderstorms, which affect the region and are filtered out on the monthly scale.

The pattern of the large-scale anomalies suggests that during the positive (negative) phases of the CCA1 the

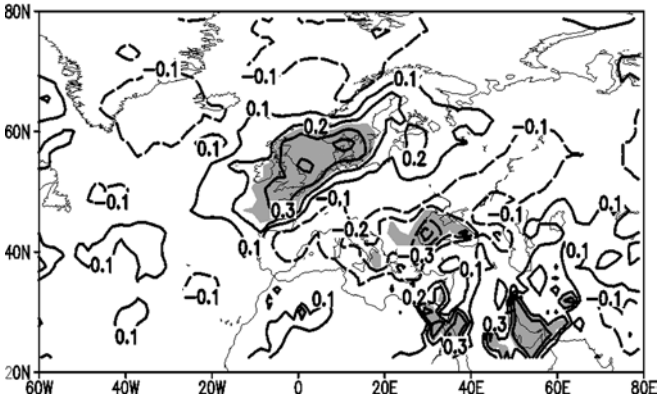

Fig. 8 Correlation fields of the first canonical air temperature series with precipitation provided by the NCEP/NCAR reanalysis for the period 1950–1999. *Shaded areas* highlight significant correlations accounting for persistence

northerly winds in the Aegean Sea are reduced (increased) in intensity, therefore allowing for higher (lower) than normal air temperatures in the area. This idea is consistent with the suggestions of other authors (Bartzokas and Metaxas 1991; Metaxas et al. 1991; Maheras and Kutiel 1999) reporting on lower air temperatures over the Aegean Sea associated with a strengthening of the northeasterlies.

As stated before, the time components of the first CCA mode (Fig. 6j) correlate very well with the weighted temperature averages in the area (Fig. 2b). It is worth pointing out that the decadal changes in the regional temperature that show positive anomalies since the beginning of the record until the mid 1960s and since the mid 1980s and cold anomalies in-between are well replicated by the variations in the first CCA. This suggests that the first CCA is responsible not only for the interannual variability of temperature on the area but also for the decadal changes mentioned and reported by various other authors (Metaxas et al. 1991; Bartzokas and Metaxas 1995; Kadıoğlu 1997; Proedrou et al. 1997; Maheras and Kutiel 1999; Türkeş et al. 2002).

5.2 Coupled CCA2 patterns between Greek summer temperature and combined large scale atmospheric and thermic fields

The second CCA pattern is connected with temperature anomalies of different signs over the Aegean Sea and over the west of Greece. These temperature anomalies are related to changes in the intensity of the zonal flow.

The pattern of the geopotential height anomalies for the second CCA component shows a zonal circulation type. High scores in this CCA correspond to summers that can be described to be of a "high index" circulation type or months in which synoptic conditions of a high index type are more frequent. For positive (negative) values of the corresponding canonical series, positive (negative) anomalies dominate in higher latitudes and negative (positive) ones over the Mediterranean. This leads to an intensified (weakened) zonal flow and a southward (northward) shift of the Subtropical Jet (300 hPa). The thickness anomalies for the three selected tropospheric layers cover similar areas of anomalies to those of geopotential heights suggesting a barotropic atmosphere. A similar type of reasoning as stated before for the cold lows and the warm blocking highs would apply here. At the surface, the station air temperatures over the area studied follow a similar configuration to that of the thickness 1000–700 hPa layer, with negative anomalies to the west of Greece and positive anomalies over the Aegean area.

For the positive phase of this CCA component, westerly to southwesterly winds supply the already warm Aegean Sea with warm air masses from Northern Africa. This is in agreement with the findings of Bartzokas and Metaxas (1991), Metaxas et al. (1991) and Maheras and Kutiel (1999). Both, the first and the second CCA components picture situations of warm (cold) temperatures over the Aegean Sea associated with southwestern (northeastern) surface winds.

The SSTs depend on a number of factors, such as radiation, vertical transport of sensible and latent heat fluxes, and horizontal and vertical sea currents. The wind speed also affects the SSTs in that it influences the sea currents and thereby the heat transport.

For both CCA components, the SSTs show a pattern that seems to follow the thickness anomaly pattern of the 1000–700 hPa layer. This suggests that in both cases, the atmosphere forces the temperature gradients on the surface of the Mediterranean Sea. An example on the local scale is the SSTs and the local sea currents in the Aegean area. The average surface currents in the Mediterranean move counter-clockwise along the coast (Weyl 1970). In fact, there is a surface inflow from the Straits of Gibraltar and, to a minor degree, from the Black Sea, due to high evaporation in the Mediterranean, which exceeds rainfall and run-off. The Gibraltar current proceeds along the North African coast and that from the Black Sea turns westward along the northern Aegean coast, after passing the Dardanelles. When a persistent air current prevails, such as the Etesian wind system over the Aegean during summer, the anti-clockwise sea current is altered and upwelling occurs along the Turkish coast (Weyl 1970). Such a situation corresponds to the negative phase both in CCA1 and CCA2, in which the intensity and/or frequency of winds with a northerly component increases. This pattern allows for upwelling and therefore results in the presence of colder water in the area. The results shown before seem to be consistent with this idea in that local negative SST anomalies appear to be related to northerly wind anomalies in the area and such effect would superimpose on the negative air temperature anomaly.

5.3 Extreme warm and cool summers in Greece

The warm and the cold summers anomaly composites (Figs. 3, 4) show different signs and eventually different details at the regional scale. However, the structure of the anomalies is similar to CCA1 as already mentioned before. This suggests that there is a unique mode of large-scale variability that allows for an extreme manifestation of the land–sea contrast and controls both warm and cold extreme states.

The extremely warm summers in Greece can be explained by the large-scale circulation patterns in Fig. 3a–d. However, it is worth discussing in more detail the local dynamical and thermal conditions that favour the high temperature anomalies. As for the positive phase of the first CCA pair, extremely high summer temperatures could be attributed to subsidence at the mid and upper troposphere, anomalous continental air from easterly directions and an enhanced advection of warm air masses originating in North Africa. These warm air masses contribute to above normal temperatures.

Over the period 1929–1999, significant warming trends have been found for mean, minimum and maximum summer temperatures of the western Aegean Turkish stations (Turkes et al. 2002). Further, summer night-time warming rates are generally stronger than those for daytime temperatures. These strong, significant warming trends in summer minimum temperatures of Turkish stations can be related to the widespread, rapid and increased urbanisation in Turkey, in addition to long-term and global effects of the human-induced climate change on air temperatures (Türkeş et al. 2002). The effect of urbanisation is apparent also in the observed upward trend of maximum and minimum air temperatures of Athens (Philandras et al. 1999). However, positive summer minimum temperature trends, though not significant, characterise the majority of the coastal and island Greek stations (not shown). It has to be stressed that these warming night-time temperature trends are found also for non-urban stations like Skiros and Milos (Aegean islands). This indicates that the upward trend of the minimum temperatures, in the area, is not only a consequence of urbanisation and is also associated with the corresponding trends in circulation modes. In addition, Arseni-Papadimitriou et al. (2000) report on the connection between the Greek maximum temperature trends with the trends of circulation types and support these findings.

The monthly spatial minimum and maximum summer temperatures for Greece and western Turkey both indicate a slight upward trend (not shown), although not significant. Nevertheless, it is interesting to note that the maximum monthly temperature increases in a much slower rate than the minimum monthly temperature, resulting in a narrowing of the monthly temperature range. However, our analysis revealed that during the extremely hot and cool summers, the maximum monthly temperatures contributed more to the rise of the monthly mean temperature than the minimum monthly temperatures (not shown). In addition, August and September contributed most to the positive and negative temperature deviations from the long-term mean. Furthermore with reference to the 1950–1999 interval, the importance of the minimum temperatures increases in August and September regarding extremely warm summers. This can be attributed to the increasing length of the night in August and September, which coincides with the annual maximum of the SSTs during these two months.

During cool summers, the anomaly composites (Fig. 4), in analogy to the negative phase of CCA1, suggest that low summer temperatures over Greece go along with enhanced instability, more cloudiness and heavy precipitation due to thunderstorms (see above).

The summer of 1976 as shown by the weighted summer mean (Fig. 2a) and the canonical time series of CCA1 (Fig. 6i) was the coolest summer of the second half of the twentieth century over the northeastern Mediterranean. However, this same summer was one of the hottest and driest in the United Kingdom (Ratcliffe 1978). The atmospheric conditions controlling this exceptional summer can be also explained by the reverse signed first canonical mode in Fig. 6, with anticyclonic conditions and pronounced stability over Western and Central Europe and cool air advection from higher latitudes via Scandinavia towards Greece. This highlights the importance of our study for the analysis of extreme cases like such an extreme summer.

5.4 CCA and cross-validation results, importance of predictors

Figure 5 shows that hindcast is best in August. During this month, the atmospheric conditions resulting from the CCA have been more frequent and play a major role on the surface air temperature over the Greek peninsula. Figure 5 and Table 1 both illustrate that the highest values of skill are reached with the SST and thickness predictors at low tropospheric levels, a reasonable feature since the SST and thickness are more closely related to temperature than circulation. As has been stated before, more than 50% of the summer temperature variability can be explained by the combined approach with eight predictor fields.

The statistical model could be improved by considering additional important predictors such as Omega fields and other kinematic fields (velocity, **u** and **v** wind vectors). In addition, other processes and factors not directly related to the state of the atmosphere, like deforestation and land use change and urbanisation, might be of importance.

6 Conclusions

The interannual and decadal summer (June–September) air temperature variability over Greece and western Turkey and its connection to the large-scale atmospheric circulation, thickness patterns and Mediterranean SSTs was investigated for the period 1950–1999.

The summer air temperature of the area is characterised by warm 1950s and 1990s and rather cool 1960s, 1970s and early 1980s. No significant linear trend was found for the individual summer months and the averaged summer temperatures over the 50-year period.

The warmest summer was in 1999, the coolest summer in 1976. August and September contribute more to temperature extremes than June and July. Furthermore, monthly maximum temperatures are more important in causing warm and cool extremes than the monthly minimum temperatures.

The large-scale variability strongly influences the variability of local temperature in parts of the eastern Mediterranean.

The CCA experiments with the combined, multicomponent large-scale predictors and summer temperature served to investigate the covariability between eight geopotential height and thermal fields and the Greek–Turkish station summer air temperature.

More than 50% of the total summer air temperature variability for 1950–1999 over Greece and western Turkey can be explained linearly by the combination of the eight large-scale predictor fields.

The most skilful predictors for the summer air temperature are the 300 hPa and 500 hPa geopotential heights, the best thermic predictors are the 1000–700 hPa thickness fields and the Mediterranean SSTs.

The first CCA pattern captures well the variability described in the composites and can therefore be assumed to be responsible for the warm (ten warmest summers) and cool (ten coolest summers) extreme temperature conditions over Greece and western Turkey and can be labelled as a "low index" circulation type. This pattern is associated with a temperature pattern in which the land–sea contrast becomes more apparent. The second CCA mode describes changes in the intensity of the zonal flow over the Atlantic and can be identified as a "high index" type of circulation in middle latitudes.

The extremely warm (cool) summers are associated with subsidence and stability (convergence and instability), anomalous advection from northeast (southwest) at the mid and upper troposphere and anomalous westerly (easterly) air flow in the lower troposphere. Further, warm (cool) extremes can be attributed to a warm (cool) troposphere over Greece as well as positive (negative) Mediterranean SSTs and decreased (increased) frequency and intensity of northerly winds in the lower troposphere.

The results shown here help to understand the variability and the extremes of the summer climate in the eastern Mediterranean area. Furthermore, implications can also be drawn regarding the climate change discussion since regional changes due to the increase of the concentrations of greenhouse gases and aerosols would be partially imposed on the large-scale by changing the intensity and frequency of the patterns described.

Acknowledgements The authors are grateful for being enabled to use monthly mean, maximum mean and minimum mean Greek station temperature series from the Greek National Meteorological Service and Turkish data from GHCN2. We also thank NCEP/NCAR for providing their reanalysis data. We are indebted to the British Meteorological Office for the preparation of the gridded SST data and literature on the warm and dry summer of 1976. We would like to thank Prof. Murat Türkeş (Turkish State Meteorological Service, Ankara, Turkey) for his very valuable help concerning Turkish temperature variability. Many thanks also go to Nicolas Schneider, Dr. Werner Eugster and Reto Burkard (University of Bern) for discussions on different aspects of the paper and to Esther Thalmann for proof reading the English text. Dr. Eleni Xoplaki was supported by the Greek State Scholarships Foundation, Dr. J. Fidel González-Rouco was partially funded by project REN-2000-0786-cli, and Dr. Jürg Luterbacher was supported by the Swiss NCCR Climate programme. The reviewers made useful comments and with their suggestions helped to improve the quality of the paper.

References

Arseni-Papadimitriou A, Maheras P, Patrikas J, Anagnostopoulou C (2000) Distribution géographique des températures maximales par type de circulation et leurs tendances, en Grèce. Publ AIC 13: 347–355

Barnett TP, Preisendorfer RW (1987) Origins and levels of monthly and seasonal forecast skill for United States air temperature determined by canonical correlation analysis. Mon Weather Rev 115: 1825–1850

Bartzokas A, Metaxas DA (1991) Climatic fluctuation of temperature and air circulation in the Mediterranean. Environment and quality of life, climate and global change. In: Proc European School of Climatology and Natural Hazards course, Arles/Rhone, France 279–297

Bartzokas A, Metaxas DA (1995) Factor analysis of some climatological elements in Athens, 1931–1992: covariability and climatic change. Theor Appl Climatol 52: 195–205

Bartzokas A, Metaxas DA, Ganas IS (1994) Spatial and temporal sea-surface temperature covariances in the Mediterranean. Int J Climatol 14: 201–213

Brown TJ, Eischeid JK (1992) An examination of spatial statistical techniques for interpolation of gridded climate data. In: Joint Proc Americ Meteorol Soc Environment Canada (eds) 12th Conf Prob Statis Atmos Sci and 5th Int Meeting Statist Climatol Toronto, Canada 739–742

Cattell RB (1966) The scree test for the number of factors. Multivar Behav Res 1: 245–276

Corte-Real J, Qian B, Xu H (1998) Regional climate change in Portugal: precipitation variability associated with large-scale atmospheric circulation. Int J Climatol 18: 619–635

Craddock JM, Flood CR (1969) Eigenvectors for representing the 500 mb geopotential surface over the Northern Hemisphere. Q J R Meteorol Soc 95: 576–593

Elsner JB, Schmertmann CP (1994) Assessing forecast skill through cross validation. Weather Forecast 9: 619–624

Giles BD, Flocas AA (1984) Air temperature variations in Greece. Part I. Persistence, trend and fluctuations. J Climatol 4: 531–539

Glahn HR (1968) Canonical correlation and its relationship to discriminant analysis and multiple regression. J Atmos Sci 25: 23–31

GNCCD (2000) First National Report on the Implementation of the United Nations Convention to combat Desertification. Greek National Committee for Combating Desertification (GNCCD). UN Convention to Combat Drought and Desertification (UNCCD). Available through: http://www.unccd.int

Gyalistras D, von Storch H, Fischlin A, Beniston M (1994) Linking GCM-simulated climatic changes to ecosystem models: case studies of statistical downscaling in the Alps. Clim Res 4(3): 167–189

Hotelling H (1935) The most predictable criterion. J Educ Psych 26: 139–142

Hotelling H (1936) Relations between two sets of variables. Biometrika 28: 321–377

Hurrell JW (1995) Decadal trends in the North Atlantic oscillation: regional temperatures and precipitation. Science 269: 676–679

Hurrell JW, van Loon H (1997) Decadal variations in climate associated with the North Atlantic Oscillation. Clim Change 36: 301–326

IPCC Climate Change (2001a) Impacts adaptation and vulnerability. Contribution of working group II to the third assessment report of the Intergovernmental Panel on Climate Change (IPCC). McCarthy JJ, Canziani OF, Leary NA, Dokken DJ, White KS (eds) Cambridge University Press, UK

IPCC Climate Change (2001b) The scientific basis. Contribution of working group I to the third assessment report of the Intergovernmental Panel on Climate Change (IPCC). Houghton JT, Ding Y, Griggs DJ, Noguer M, Van der Linden PJ, Xiaosu D (eds) Cambridge University Press, UK

IPCC Emissions Scenarios (2000) Emissions scenarios. Special report of the Intergovernmental Panel on Climate Change. Nakicenovic N, Swart R (eds) Cambridge University Press, UK

IPCC Policy Makers (2001) Summary for policy makers. A report of Working Group I of the Intergovernmental Panel on Climate

Change. Albritton DL et al. (eds) Available through: http://www.ipcc.ch/pub/spm22-01.pdf
IPCC Technical Summary (2001) Technical summary. Climate change 2001: impacts, adaptation, and vulnerability. A Report of Working Group II of the Intergovernmental Panel on Climate Change. White KS et al. Manning M (New Zealand), Nobre C (Brazil) (eds), Cambridge University Press, UK, pp 21–73
Kadıoğlu M (1997) Trends in surface air temperature data over Turkey. Int J Climatol 17: 511–520
Kaiser HF (1960) The application of electronic computers to factor analysis. Educational and psychological measurement 20: 141–151
Kalnay E et al. (1996) The NCEP/NCAR 40-Year Reanalysis Project. Bull Am Meteorol Soc 77: 437–471
Katsoulis BD, Theoharatos GA (1985) Indications of the urban heat island in Athens, Greece. J Clim Appl Meteorol 24: 1296–1302
Kier FJ (1997) Ways to explore the replicability of multivariate results (since statistical significance testing does not). Annual Meeting of the Southwest Research Association, Austin. Available through: http://academic.son.wisc.edu/rdsu/pdf/replication.pdf
Kistler E et al. (2001) The NCEP/NCAR 50-Year Reanalysis: monthly means CD-ROM and documentation. Bull Am Meteorol Soc 82: 247–267
Kovats RS, Haines A, Stanwell-Smith E, Martens P, Menne B, Bertollini R (1999) Climate change and human health in Europe. Brit Med J 318: 1682–1685
Kutiel H, Maheras P (1998) Variations in the temperature regime across the Mediterranean during the last century and their relationship with circulation indices. Theor Appl Climatol 61: 39–53
Levine MS (1977) Canonical analysis and factor comparison. Thousand Oaks, Sage Publication, Quantitative Applications in the Social Sciences Series 6
Livezey RE (1995) The evaluation of forecasts. In: von Storch H, Navarra A (eds) Analysis of climate variability. Springer, Berlin Heidelberg New York, pp 177–196
Livezey RE, Smith TM (1999a) Considerations for use of the Barnett and Preisendorfer (1987) algorithm for canonical correlation analysis of climate variations. J Clim 12: 303–305
Livezey RE, Smith TM (1999b) Covariability of aspects of North American climate with global sea surface temperatures on interannual to interdecadal timescales. J Clim 12: 289–302
Lolis CJ, Bartzokas A, Metaxas DA (1999) Spatial covariability of the climatic parameters in the Greek area. Int J Climatol 19: 185–196
Maheras P, Kutiel H (1999) Spatial and temporal variations in the temperature regime in the Mediterranean and their relationship with circulation during the last century. Int J Climatol 19: 745–764
Maheras P, Kutiel H, Vafiadis M (1998) Tendances spatiales et temporelles de la pression atmosphérique de surface et des géopotentieles de 500 hPa en Europe et en Méditerranée durant la dernière période 1950–1994. Publ AIC 11: 345–351
Maheras P, Xoplaki E, Davies TD, Martin-Vide J, Bariendos M, Alcoforado MJ (1999) Warm and cold monthly anomalies across the Mediterranean and their relationship with circulation; 1860–1990. Int J Climatol 19: 1697–1715
Maheras P, Flocas HA, Patrikas I, Anagnostopoulou C (2001) A 40 year objective climatology of surface cyclones in the Mediterranean region: spatial and temporal distribution. Int J Climatol 21: 109–130
Matzarakis A (1999) Required meteorological and climatological information for tourism. In: Proc 15th Int Congress of Biometeorology & International Conference on Urban Climatology, de Dear RJ, Potter JC (eds) ICBPO8.01: 1–6
Metaxas DA, Bartzokas A, Vitsas A (1991) Temperature fluctuations in the Mediterranean area during the last 120 years. Int J Climatol 11: 897–908
Michaelsen J (1987) Cross-validation in statistical climate forecast models. J Clim Appl Meteorol 26: 1589–1600
Mitchell TD, Hulme M, New M (2002) Climate data for political areas. Area 34: 109–112
Namias J (1948) Evolution of monthly mean circulation and weather patterns. Trans Amer Geophys U 29: 777–788
North GR, Bell TL, Cahalan RF, Moeng FJ (1982a) Sampling errors in the estimation of empirical orthogonal functions. Mon Weather Rev 110: 699–706
North GR, Moeng FJ, Bell TL, Cahalan RF (1982b) The latitude dependence of the variance of zonally averaged quantities. Mon Weather Rev 110: 319–326
Peterson TC, Vose RS (1997) An overview of the global historical climatology network temperature Database. Bull Am Meteorol Soc 78: 2837–2849
Peterson TC, Vose R, Schmoyer R, Razuvaëv V (1998) Global historical climatology network (GHCN) quality control of monthly temperature data. Int J Climatol 18: 1169–1179
Philandras CM, Metaxas DA, Nastos PT (1999) Climate variability and urbanization in Athens. Theor Appl Climatol 63: 65–72
Preisendorfer RW (1988) Principal component analysis in meteorology and oceanography. Developments in Atmospheric Sciences 17. Elsevier, Amsterdam, pp 293–318
Preisendorfer RW, Zwiers FW, Barnett TP (1981) Foundations of principal component selection rules. SIO Ref Ser 81-4, Scripps Institution of Oceanography, La Jolla, CA, USA
Proedrou M, Theoharatos G, Cartalis C (1997) Variations and trends in annual and seasonal air temperatures in Greece determined from ground and satellite measurements. Theor Appl Climatol 57: 65–78
Ratcliffe RAS (1978) Meteorological aspects of the 1975–1976 drought. Proc R Soc London A 363: 3–20
Rayner NA, Horton EB, Parker DE, Folland CK, Hackett RB (1996) Version 2.2 of the Global sea-Ice and Sea Surface Temperature data set, 1903–1994. CRTN 74. Available from Hadley Centre Met Office Bracknell, UK
Reddaway JM, Bigg GR (1996) Climatic change over the Mediterranean and links to the more general atmospheric. Int J Climatol 16: 651–661
Ribera P, Garcia R, Diaz HF, Gimeno L, Hernandez E (2000) Trends and interannual oscillations in the main sea-level surface pressure patterns over the Mediterranean, 1955–1990. Geophys Res Lett 27: 1143–1146
Sahsamanoglou HS, Makrogiannis TJ (1992) Temperature trends over the Mediterranean region, 1950–1988. Theor Appl Climatol 45: 183–192
Schönwiese CD, Rapp J, Fuchs T, Denhard M (1994) Observed climate trends in Europe 1891–1990. Meteorol Z NF 3: 22–28
Schönwiese CD, Walter A, Rapp J, Meyhöfer S, Denhard M (1998) Statistische Analyse der Klimavariabilität und anthropogenen Klimasignale in globaler und regionaler Betrachtung. Ber Inst Meteor und Geophys Univers Frankfurt/Main 102. Eigenverlag des Instituts, Frankfurt/Main
Slonosky VC, Yiou P (2002) Does the NAO index represent zonal flow? The influence of the NAO on North Atlantic surface temperature. Clim Dyn 19: 17–30
Slonosky VC, Jones PD, Davies TD (2001) Atmospheric circulation and surface temperature in Europe from the 18th century to 1995. Int J Climatol 21: 63–75
Smith TM, Livezey RE (1999) GCM systematic error correction and specification of the seasonal mean Pacific-North America region atmosphere from global SSTs. J Clim 12: 273–288
Tayanç M, Karaca M, Yenigün O (1997) Annual and seasonal air temperature trend patterns of climate change and urbanization effects in relation to air pollutants in Turkey. J Geophys Res 102: 1909–1919
Trenberth KE, (1990) Recent observed interdecadal climate changes in the Northern Hemisphere. Bull Am Meteorol Soc 71: 989–993
Trenberth KE (1995) Atmospheric circulation climate changes. Clim Change 31: 427–453

Türkeş M, Sümer UM, Kılıç G (1995) Variations and trends in annual mean air temperatures in Turkey with respect to climatic variability. Int J Climatol 15: 557–569

Türkeş M, Sümer UM, Demir İ (2002) Re-evaluation of trends and changes in mean, maximum and minimum temperatures of Turkey, for the period 1929–1999. Int J Climatol 22: 947–977

von Storch H, Zwiers FW (1999) Statistical analysis in climate research. Cambridge University Press, UK

Vose RS, Schmoyer RL, Steurer PM, Peterson TC, Heim R, Karl TR, Eischeid J (1992) The global historical climatology network: long-term monthly temperature, precipitation, sea level pressure, and station pressure data. ORNL/CDIAC-53, NDP-041. Carbon Dioxide Information Analysis Center, Oak Ridge National Laboratory, Oak Ridge, Tennessee

Wanner H, Rickli R, Salvisberg E, Schmutz C, Schüepp M (1997) Global climate change and variability and its influence on Alpine climate – concepts and observations. Theor Appl Climatol 58: 221–243

Ward MN, Folland CK (1991) Prediction of seasonal rainfall in the north Nordeste of Brazil using eigenvectors of sea-surface temperature. Int J Climatol 11: 711–743

Welch BL (1937) The significance of the difference between two means when the population variances are unequal. Biometrika 29: 350–362

Weyl PK (1970) Oceanography, an introduction to the marine environment. Sons, New York

Wilks DS (1995) Statistical methods in the atmospheric sciences: an introduction. International Geophysics Series vol 59. Academic Press, New York

Xoplaki E (2002) Climate variability over the Mediterranean. PhD thesis, University of Bern, Switzerland (http://sinus.unibe.ch/klimet/docs/phd_xoplaki.pdf)

Xoplaki E, Luterbacher J, Burkard R, Patrikas I, Maheras P (2000) Connection between the large scale 500 hPa geopotential height fields and precipitation over Greece during wintertime. Clim Res 14: 129–146

Yarnal BM, Diaz HF (1986) Relationship between extremes of the Southern Oscillation and the winter climate of the Anglo-american Pacific coast. J Climatol 6: 197–219